Ferromagnetic HfO$_2$/Si/GaAs interface for spin-polarimetry applications

O. E. Tereshchenko, V. A. Golyashov, S. V. Eremeev, I. Maurin, A. V. Bakulin, S. E. Kulkova, M. S. Aksenov, V. V. Preobrazhenskii, M. A. Putyato, B. R. Semyagin, D. V. Dmitriev, A. I. Toropov, A. K. Gutakovskii, S. E. Khandarkhaeva, I. P. Prosvirin, A. V. Kalinkin, V. I. Bukhtiyarov, and A. V. Latyshev

Ferromagnetic HfO₂/Si/GaAs interface for spin-polarimetry applications

O. E. Tereshchenko,[1,2,a)] V. A. Golyashov,[1,2] S. V. Eremeev,[3,4] I. Maurin,[5] A. V. Bakulin,[3]
S. E. Kulkova,[3,4] M. S. Aksenov,[1] V. V. Preobrazhenskii,[1] M. A. Putyato,[1] B. R. Semyagin,[1]
D. V. Dmitriev,[1] A. I. Toropov,[1] A. K. Gutakovskii,[1,2] S. E. Khandarkhaeva,[2] I. P. Prosvirin,[6,2]
A. V. Kalinkin,[6] V. I. Bukhtiyarov,[6,2] and A. V. Latyshev[1,2]

[1]Rzhanov Institute of Semiconductor Physics, Novosibirsk 630090, Russian Federation
[2]Novosibirsk State University, Novosibirsk 630090, Russian Federation
[3]Institute of Strength Physics and Materials Science, 634021 Tomsk, Russian Federation
[4]Tomsk State University, 634050 Tomsk, Russian Federation
[5]Laboratoire de Physique de la Matière Condensée, Ecole Polytechnique - CNRS, 91128 Palaiseau Cedex,
France
[6]Boreskov Institute of Catalysis, Novosibirsk 630090, Russian Federation

In this letter, we present electrical and magnetic characteristics of HfO₂-based metal-oxide-semiconductor capacitors (MOSCAPs), along with the effect of pseudomorphic Si as a passivating interlayer on GaAs(001) grown by molecular beam epitaxy. Ultrathin HfO₂ high-k gate dielectric films (3–15 nm) have been grown on Si/GaAs(001) structures through evaporation of a Hf/HfO₂ target in NO₂ gas. The lowest interface states density D_{it} at Au/HfO₂/Si/GaAs(001) MOS-structures were obtained in the range of $(6 - 13) \times 10^{11}$ eV^{-1} cm^{-2} after annealing in the 400–500 °C temperature range as a result of HfO₂ crystallization and the Si layer preservation in non-oxidized state on GaAs. HfO₂-based MOSCAPs demonstrated the ferromagnetic properties which were attributed to the presence of both cation and anion vacancies according to the first-principle calculations. Room-temperature ferromagnetism in HfO₂ films allowed us to propose a structure for the ferromagnetic MOS spin-detector. © 2015 AIP Publishing LLC.
[http://dx.doi.org/10.1063/1.4931944]

The creation of metal-insulator-semiconductor (MIS) structures in which both insulator and metal layers are ferromagnetic could be very promising for spin polarimetry applications based on the optical detection of spin-filter effect[1,2] and spin-dependent transistors.[3,4] Injection of spin-polarized electrons into semiconductors is the first step towards the realization of semiconductor-based spintronic devices which utilize the spin degree of freedom of electrons. Herewith, the insulator layers (tunneling barriers) and interfaces play the crucial role in the scattering mechanisms of charge and spin that require the control of electrical and ferromagnetic (FM) properties of MIS junctions to achieve efficient spin-injection and spin detection in spintronic devices.[2]

Thin insulating films on semiconductors are of current interest regarding the applications using electron tunneling between ferromagnetic films and semiconductors. Hafnium oxide (HfO₂) has been extensively studied during the last years due to its relatively high dielectric constant, high melting point, and chemical stability. It is found suitable as a high-k material to replace the gate dielectrics in field effect transistors and dynamic random access memories.[5] HfO₂ is particularly interesting because it can be grown on Si surfaces with a low density of interface states, while Si itself can be grown pseudomorphic on a GaAs surface forming the so-called interface control layer (ICL).[6–8] Moreover, HfO₂ demonstrated the room temperature ferromagnetism.[9] The observation of ferromagnetism in un-doped HfO₂ has opened up a possibility to use this compound in magneto-optic and

magneto-electronic applications. The modulation of pure spin currents with a ferromagnetic insulator has been recently demonstrated.[10] In this respect, a three layer system of FM metal/FM insulator/semiconductor (FMM/FMI/S) could be used as a spin selective filter with self-calibrated properties.[11] Schematically, the proposed GaAs-based FM MIS structure is shown in Fig. 1. The proposed structure should allow to measure all three spin components: two in-plane components, by measuring cathodoluminescence intensity,[1] and out of plane component by measuring the cathodoluminescence polarization.[12]

The present research work reports experimental data on the epitaxial growth, composition, electrical and magnetic properties of thin HfO₂ films deposited by electron beam evaporation of the Hf/HfO₂ target in an NO₂ flux. The reactions between HfO₂ and Si/GaAs during deposition and
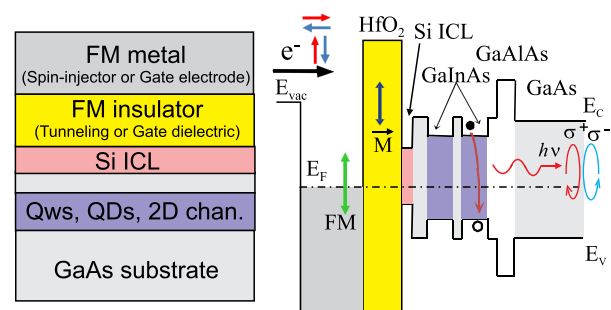

FIG. 1. The proposed MOS-structure (left) and a band diagram of Si ICL passivated GaAs-based structure with both FM base (gate) electrode and FM tunneling insulator layer (right).

a)Electronic mail: teresh@isp.nsc.ru

post-annealing have been studied to promote the HfO_2 layer crystallization and to obtain the best electrical results.

The investigated structures were prepared in three stages. First, the Si/GaAs structures were grown by molecular beam epitaxy (MBE) in ultrahigh vacuum (UHV) system with the base pressure of 3×10^{-10} Torr. The epi-ready GaAs(001) wafer was cleaned by heating in an As flux to remove the surface oxide followed by 0.7 μm buffer and 0.3 μm channel n-type GaAs layers (Si-doped to 1×10^{18} cm^{-3} and 3×10^{16} cm^{-3}, respectively) grown at $T_s = 580\,°C$. Then the substrate was cooled down to $500\,°C$ in the As ambient to form a $\beta 2(2 \times 4)$ surface structure. As the arsenic residual pressure reached the background level, the substrate temperature was raised to $\sim 550\,°C$ and the transition from (2×4) to (3×1) reconstruction was observed. In few minutes, when the As pressure lowered to the background level, 0.5 atomic layer (AL) of Ga was deposited onto the (3×1) surface to form a Ga-rich (4×6) or (2×6) surface structure for further Si deposition. Si deposition led to the sequence of surface reconstructions: (4×2) at ~ 0.3 Si AL with a subsequent transition and stabilization of the (1×2) structure, shown in Figure 2(a). After 6 ALs of Si, the substrate was cooled down to room temperature, and ~ 100 nm of elemental arsenic were deposited to preserve the surface from oxidation and contamination during transportation to the HfO_2 deposition chamber.

At the second stage, the As/Si/GaAs samples were transferred through the air to UHV sample preparation chamber of a photoelectron spectrometer (SPECS). The samples were annealed during 30 minutes at $T_s \sim 450–480\,°C$ to desorb the protective As layer. The hafnium oxide layers were deposited in the preparation chamber of an electron spectrometer on the Si/GaAs surface by e-beam evaporation of HfO_2/Hf target in the NO_2 and O_2 ambient ($P_{NO_2} \sim 1 \times 10^{-6}$ Torr) produced through the decomposition of lead (II) nitrate $Pb(NO_3)_2$ by heating in vacuum: $3Pb(NO_3)_2 \rightarrow Pb_3O_4\downarrow + 6NO_2\uparrow + O_2\uparrow$.[13] The HfO_2 deposition rate was about 3 nm per hour. The chemical composition of deposited layers was studied by XPS using SPECS spectrometer with the PHOIBOS-150-MCD-9 hemispherical energy analyzer and X-ray monochromator

FOCUS-500 (AlK irradiation, $h\nu = 1486.74$ eV, 200 W). Surface morphology was studied by AFM (Solver P-47H) in semicontact topographic regime. The results of AFM studies showed that HfO_2 films had a slightly pronounced relief with a height peak-to peak difference in the range of $\sim 0.2–0.4$ nm with the root-mean-square (rms) roughness on the 5×5 μm^2 area equal to 0.21 nm. The roughness of initial Si/GaAs surface was about 0.15 nm. Thus, HfO_2 deposition did not lead to a significant increase in surface roughness.

At the third stage, the MIS-structures were formed by the deposition of gold or In_2O_3 electrodes on the HfO_2/Si/GaAs structure to study the electrical properties. The InGa eutectic was used to form a back-ohmic contact to GaAs. The Au/HfO_2/Si/GaAs MIS-structures were studied by the standard high-frequency C-V method ($f \sim 10 - 100$ kHz). The magnetization measurements were carried out at room temperature employing a cryogenic SX600 superconducting quantum interference device magnetometer.

The cross-sectional high-resolution transmission electron microscopy (HRTEM) images of HfO_2/Si/GaAs, as a function of the annealing conditions, are shown in Figs. 2(c) and 2(d). The as-deposited HfO_2 films were mostly amorphous and partly transformed to a polycrystalline with a monoclinic structure after annealing at $350\,°C$ [Fig. 2(c)]. The monoclinic crystalline structures were confirmed using the fast Fourier transformation (FFT) of the HRTEM image. The interfacial layer with 1.5–1.7 nm thickness is a little thicker to be regarded as a Si passivation layer only and consists of a pure crystalline Si layer (≤ 0.9 nm) and an amorphous transitional Si-Hf-O layer (~ 0.7 nm) caused by the annealing process. The formation of mixed Si layer with Hf at the interfacial region after annealing was confirmed by the observation of the chemical shift in Si2p line [Fig. 3(d)]. Annealing at $450\,°C$ led to the complete crystallization of HfO_2 layer, increasing the disordered Si-Hf-O layer thickness and decreasing the crystalline Si layer thickness [Fig. 2(d)]. Annealing above T $= 500\,°C$ amorphized the transitional layer forming a disordered Si-Hf-O layer along with the GaAs oxidation and degradation of electrical properties.
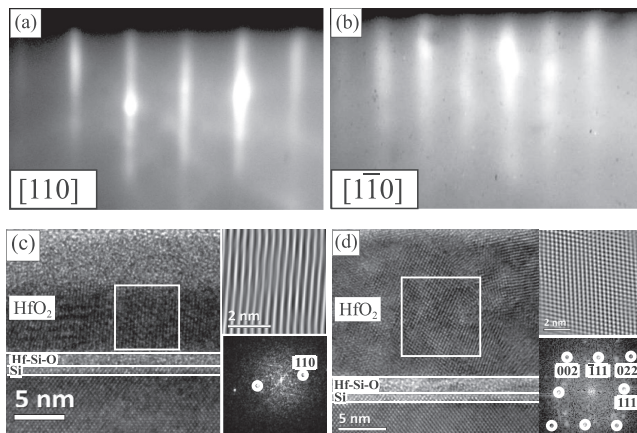

FIG. 2. Reflection high-energy electron diffraction patterns of the (1×2) reconstruction obtained after 6 Si ALs deposition on the (4×6)-GaAs(001) surface (a) and (b). HRTEM images of HfO_2/Si/GaAs structures as a function of annealing at $350\,°C$ (c) and $450\,°C$ (d). The zoom of the filtered square region marked at (c) and (d) and its FFT images are shown on the right sides of (c) and (d).
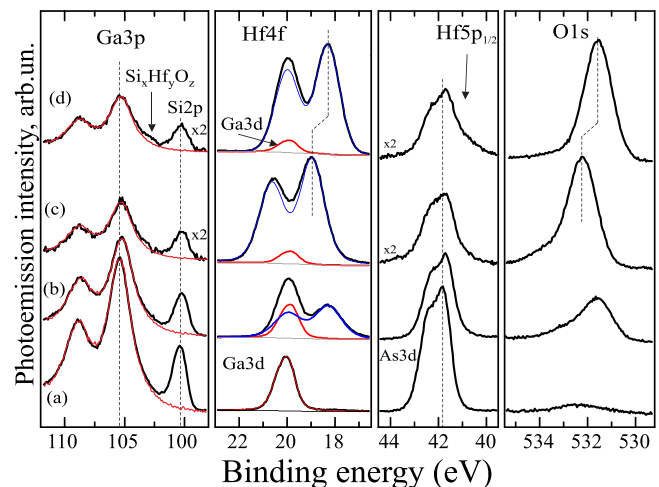

FIG. 3. XPS spectra of Si2p and Ga3p, Hf4f and Ga3d, As3d and Hf5p, and O1s for GaAs(001) surface passivated with 6 AL of Si after As decapping (a) followed by deposition of 1 nm (b) and 3 nm (c) of HfO_2 and subsequent annealing at $450\,°C$ for 20 min (d).

The XPS experiments were carried out to investigate the chemical reaction and band aliment between HfO_2 and the Si/GaAs interface. The changes in the XPS spectra of Ga3p, Si2p, Ga3d, As3d, and O1s core level (CL) spectra of as-grown and post annealed HfO_2/GaAs with the Si passivation are shown in Fig. 3. The initial Si/GaAs surface shows no traces of oxides and elemental arsenic that means the As-cap layer protected the surface from oxidation and was completely desorbed during annealing. The Si2p line has binding energy (BE) 100.5 eV which corresponds to the Si-Si bond. The BE of Si core levels in SiO_2 is chemically shifted by about 3 eV to a higher BE and can be visible only like a "shoulder" on the Ga3p line. Figs. 3(c) and 3(d) demonstrate that the deposition of HfO_2 and subsequent annealing of the HfO_2/Si/GaAs interface in UHV above 400 °C led to the appearance of a chemically shifted Si component in the energy range of 102–103 eV caused by the $Hf_xSi_yO_z$ interfacial layer formation. Another effect of the HfO_2/Si/GaAs annealing was Hf4f and O1s lines shift to low binding energies [Fig. 3(d)] by about 1 eV, whereas the substrate CLs remained at the same energy. Such behavior can be associated with the structural phase transition in HfO_2 film [Figs. 2(c) and 2(d)] and as a result with the reduction of the charging effect in HfO_2 during XPS measurements.

To determine the interface passivation properties of the Si layer, the C-V and conductivity-voltage (G/ω-V) characteristic of Au/HfO_2/6 AL Si/GaAs MIS structures were studied. Fig. 4 shows a typical C-V (a) and I-V (b) curves of Au/10 nm HfO_2/6 AL Si/n-GaAs MIS structures with an abrupt HfO_2/Si interface as a function of post-annealing temperatures. One can see that no capacity modulation is observed in the structure formed at room temperature. Such behavior can be explained by the Fermi level pinning or, more likely, by the presence of a negative built-in charge in the insulator layer shifting the flat band voltage V_{fb} above the HfO_2 electrical breakdown voltage. This agrees with the assumption that low-temperature amorphous HfO_2 films are highly defective with a high density of oxygen vacancies which trap electrons. After MIS-structures annealing at 350 °C in the argon atmosphere, the V_{fb} shifted to the value of $V_{fb} \sim 2$ V. The parallel shift to the positive voltage of the whole C-V curve indicates the presence of a negative fixed charge (Q_{fix}) located in the HfO_2 and interfacial layers. The increase in the annealing temperature to 450 °C led to a further fixed charge density reduction. The negative fixed charge in the
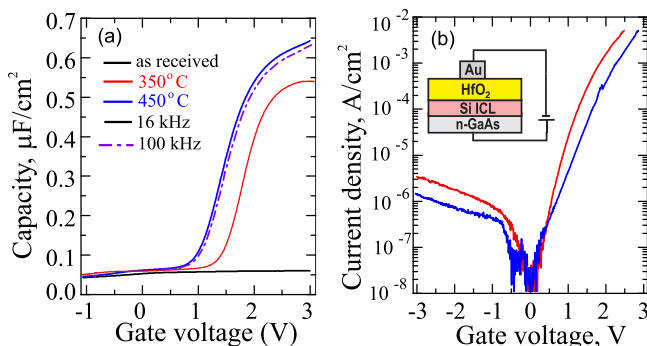
HfO_2 layer reduced drastically upon the phase transition to the monoclinic structure [Fig. 2(d)]. This can be attributed to the decrease of oxygen vacancies and the appearance of Hf vacancies. For the MIS-structure annealed at 450 °C, the density of trapped charge in HfO_2 can be evaluated as $Q_{fix} \simeq 10^{12}$ cm^{-2}. The insulating layer capacity increased by 20%; that means raising the HfO_2 dielectric susceptibility caused by the structural phase transition from amorphous HfO_2 to the monoclinic phase with a change of the dielectric constant from 12 to 16. The C-V curves demonstrate that the MIS-structure with the Si ICL has a small frequency dispersion in the range of 10–100 kHz. The density of interface states $D_{it} \simeq 6 \times 10^{11}$ eV^{-1} cm^{-2} was estimated from the value of the peak conductance in the G/ω dependence. The leakage current density through the investigated MIS-structures did not significantly depend on the annealing temperature and was $\sim 3 \times 10^{-6}$ A cm^{-2} at 1 V.

The valence band spectra of the HfO_2/Si/GaAs interface are shown in Figs. 5(a)–5(c). The valence band maximum (VBM) at the Si/GaAs surface lies at energy 0.9 eV [Fig. 5(a)] corresponding to the surface potential at $\varphi_s \simeq 0.4$ eV, whereas typical surface potential values for the n-GaAs(001) surface lie in the range of 0.6–0.9 eV. After deposition of 3 nm HfO_2, the valence band spectrum consists of both Si/GaAs and HfO_2 contributions, where HfO_2 valence states appear as a broad peak with maximum of intensity at ~ 7.5 eV [Fig. 5(b)]. Similar to the Hf and oxygen CLs shifts after annealing, the VB spectrum shows the threshold shift only in a HfO_2 film [Fig. 5(b) dotted curve]. One can conclude about the homogeneous charging of the HfO_2 film and the possibility of an artificial change of the interface band offset between the insulator and semiconductor. After the deposition of the HfO_2 film of 11 nm thickness, contribution from the GaAs substrate in the VB spectrum is almost vanished, and the VBM is shifted up to 3.9 eV below the Fermi level. The observed VB offset at the HfO_2/Si/GaAs interface is in a good agreement with the early measured offset between HfO_2 and Si, and GaAs.[14] The band diagram of the HfO_2/Si/GaAs structure extracted from the XPS and C-V analysis is shown in Fig. 5(d).

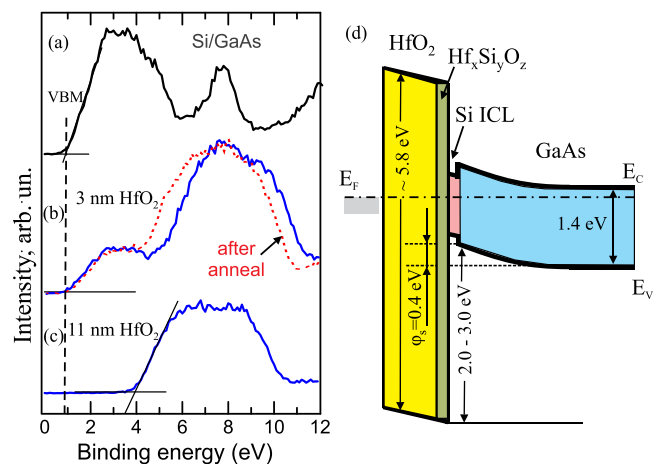FIG. 4. The measured C-V (a) and I-V (b) curves for Au/10 nm HfO_2/6 AL Si/n-GaAs MIS structures.

FIG. 5. Valence band XPS spectra from the GaAs(001) surface passivated with 6 AL of Si (a), after 3 nm deposition of HfO_2 and a subsequent annealing (dotted curve) (b) and after 11 nm deposition of HfO_2 (c). (d) A band diagram for the Au/HfO_2/Si/GaAs structure.

Since the HfO_2 ferromagnetic properties have already been demonstrated, it would be interesting to test the magnetic properties of the HfO_2/Si/GaAs interface. The magnetization measurements, shown in Fig. 6(a), evidence their room temperature (RT) ferromagnetism and clearly demonstrate that the undoped HfO_2 film is ferromagnetic with a Curie temperature above RT. The films show the coercivity of 10–30 mT at RT and remanence of the 15–20% of saturation. The saturated magnetic moment of about $\simeq 1.2 \times 10^{-8}$ Am^2 ($\simeq 200$ μ_B nm^{-2} in terms of the film area) is in a good agreement with the previous finding in HfO_2 films grown on the Si surface.[15]

To explain the nature of the observed ferromagnetism in the HfO_2/Si/GaAs structure, we performed density functional theory (DFT) calculations within the projector augmented wave method[16] with the generalized gradient approximation (GGA-PBE) for the exchange correlation term, as implemented in Vienna *Ab-initio* Simulation Package plane-wave code (VASP).[17] The monoclinic structure of HfO_2 is used since it is the structure observed in the experiment. In the calculations, a $2 \times 2 \times 2$ supercell, which contains 96 atoms, is used. For this supercell, a $2 \times 2 \times 2$ Monkhorst-Pack k-point mesh is used in the total energy calculations. For the simulation of the Hf(O) deficient system, one or two Hf(O) atoms are replaced by vacancies in the supercell. In all cases, the systems are relaxed until the forces are smaller than 0.05 eV/nm.

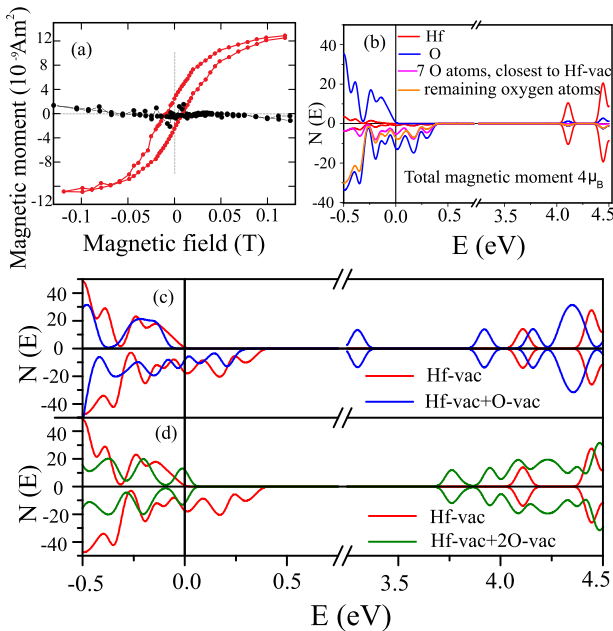In monoclinic HfO_2, each Hf atom is surrounded by seven O atoms, out of which three atoms are threefold- and four atoms are fourfold-coordinated by Hf atoms. In the perfect crystal, the O-p states are fully occupied and form the bulk valence band edge. As far as hafnium in HfO_2 is a Hf^{+4} cation, the removal of a neutral Hf atom introduces four empty states. One single Hf vacancy (that correspond to $\sim$3% of vacancies at the Hf sublattice in our supercell) introduces unoccupied but the spin-polarized states above the valence band. As one can see in Fig. 6(b), the valence band is a spin split, with the compensating holes confined to the spin-down oxygen states resulting in a half metallic ground state. The four empty states introduced by the Hf vacancy account for the calculated local magnetic moment of 4 μ_B, in accordance with the earlier calculations.[18,19] Almost half of the spin-down density of states at the Fermi level comes from the oxygen atoms surrounding the vacancy, which results in the magnetic moment of 1.88 μ_B, localized on these atoms. Wherein, the threefold-coordinated O atoms have the magnetic moments of 0.485 μ_B and fourfold-coordinated oxygen atoms give only 0.106 μ_B. The formation of the second Hf vacancy (we introduce it as far away from the first vacancy, as it is allowed by the supercell size—in our case the shorter distance between the vacancies is $\sim$0.85 nm) leads to the vacancy concentration increase up to $\sim$6%. This gives rise to an increase in the total magnetic moment of the supercell up to 8 μ_B. At the same time, the energy difference between ferromagnetic and nonmagnetic states increases with the increasing Hf vacancies concentration in favor of the ferromagnetic state that provides evidence of the stability of Hf-vacancy-induced magnetism in HfO_2.

We also considered one and two oxygen vacancies in the supercell, placing them far from the Hf vacancy and from each other. As can be seen in Fig. 6(c), the introduction of one vacancy in the system reduces the spin-down density of states twice at E_F resulting in halving the magnitude of the supercell total magnetic moment, while the supercell with a Hf vacancy and two non-interacting O vacancies [Fig. 6(d)] becomes nonmagnetic. Thus, the total magnetic moment of the cell is controlled by both Hf and O vacancies concentration.

In summary, the electric and magnetic properties of HfO_2/GaAs(001) structures with the 6 AL-thick pseudomorphic passivating silicon interlayer were studied in an attempt to create a ferromagnetic insulator/GaAs interface with a low interface state defect density for spin-filtering device application. The MIS-structures were fabricated by evaporation of Hf in the NO_2 ambient onto Si layers grown by MBE on the Ga-rich (4×6) reconstructed GaAs(001) surface. Irrespective of the HfO_2 deposition conditions, the formation of the Hf-Si-O_x transition layer at the HfO_2/Si boundary was observed after annealing. The estimated density of interface states at the Au/HfO_2/Si/n-GaAs(001) MIS-structures was in the range of $6 \times 10^{11} - 3 \times 10^{12}$ eV^{-1} cm^{-2}. The HfO_2-based MIS structures demonstrated the ferromagnetic properties with a saturation magnetic moment of $\simeq 1.2 \times 10^{-8}$ A m^2 ($\simeq 200$ μ_B nm^{-2}) and the coercive field of $\sim$10 mT. The DFT calculations showed that, in HfO_2, the charged Hf vacancies were responsible for the arising ferromagnetic state. The total magnetic moment in the supercell, which distributes mainly on the p orbitals of the oxygen atoms closest to the Hf

FIG. 6. (a) Magnetization versus magnetic field taken at RT for an Au/14 nm HfO_2/6 AL Si/n-GaAs structure before (black dots) and after annealing at 450 °C (red dots). The field was applied parallel to the film plane. The background slope is defined by the data in the range 3–5 T. (b) The spin-resolved density of states $N(E)$ projected on Hf and O atoms for the HfO_2 supercell with the Hf vacancy. The summarized partial densities of states for oxygen atoms, closest to the Hf vacancy and for the remaining 57 oxygen atoms in the $2 \times 2 \times 2$ supercell are also shown. The positive and negative values of $N(E)$ correspond to spin-majority and spin-minority states, respectively. (c) and (d) The spin-resolved total density of states $N(E)$ for the HfO_2 supercell with the Hf vacancy compared to the Hf-deficient system with one (c) and two (d) O vacancies.

vacancy, depends also on the oxygen vacancy concentration that provides the electron doping of the system.

[1] X. Li, O. E. Tereshchenko, S. Majee, G. Lampel, Y. Lassailly, D. Paget, and J. Peretti, Appl. Phys. Lett. **105**, 052402 (2014).

[2] O. E. Tereshchenko, D. Lamine, G. Lampel, Y. Lassailly, X. X. Li, D. Paget, and J. Peretti, J. Appl. Phys. **109**, 113708 (2011).

[3] S. Datta and B. Das, Appl. Phys. Lett. **56**, 665 (1990).

[4] H. C. Koo, J. H. Kwon, J. Eom, J. Chang, S. H. Han, and M. Johnson, Science **325**, 1515 (2009).

[5] J. Robbertson, Rep. Prog. Phys. **69**, 327 (2006).

[6] H. Hasegawa and M. Akazawa, Appl. Surf. Sci. **254**, 8005 (2008).

[7] D. J. Webb, J. Fompeyrine, S. Nakagawa, A. Dimoulas, C. Rossel, M. Sousa, R. Germann, S. F. Alvarado, J. P. Locquet, C. Marchiori, H. Siegwart, A. Callegari, E. Kiewra, Y. Sun, J. De Souza, and N. Hoffmann, Microelectron. Eng. **84**, 2142 (2007).

[8] S. H. Park, Yu S. Kang, J. Chae, H. J. Kim, M. H. Cho, D. H. Ko, Y. C. Byun, H. Kim, S. W. Cho, Ch. Y. Kim, and J. H. Seo, Appl. Surf. Sci. **283**, 375 (2013).

[9] M. Venkatesan, C. B. Fitzgerald, and J. M. D. Coey, Nature (London) **430**, 630 (2004).

[10] E. Villamor, M. Isasa, S. Vélez, A. Bedoya-Pinto, P. Vavassori, L. E. Hueso, F. S. Bergeret, and F. Casanova, Phys. Rev. B **91**, 020403(R) (2015).

[11] C. Cacho, Y. Lassailly, H.-J. Drouin, G. Lampel, and J. Peretti, Phys. Rev. Lett. **88**, 066601 (2002).

[12] V. L. Alperovich, A. S. Terekhov, A. S. Jaroshevich, G. Lampel, Y. Lassailly, J. Peretti, N. Rougemaille, and T. Wirth, Nucl. Instrum. Methods Phys. Res. A **536**, 302 (2005).

[13] V. A. Golyashov, K. A. Kokh, S. V. Makarenko, K. N. Romanyuk, I. P. Prosvirin, A. V. Kalinkin, O. E. Tereshchenko, A. S. Kozhukhov, D. V. Sheglov, S. V. Eremeev, S. D. Borisova, and E. V. Chulkov, J. Appl. Phys. **112**, 113702 (2012).

[14] V. V. Afanasev, H.-Y. Chou, M. Houssa, A. Stesmans, L. Lamagna, A. Lamperti, A. Molle, B. Vincent, and G. Brammertz, Appl. Phys. Lett. **99**, 172101 (2011).

[15] J. M. D. Coey, M. Venkatesan, P. Stamenov, C. B. Fitzgerald, and L. S. Dorneles, Phys. Rev. B **72**, 024450 (2005).

[16] P. E. Blöchl, Phys. Rev. B **50**, 17953 (1994).

[17] G. Kresse and J. Hafner, Phys. Rev. B **48**, 13115 (1993).

[18] J. Osorio-Guillén, S. Lany, S. V. Barabash, and A. Zunger, Phys. Rev. B **75**, 184421 (2007).

[19] H. Weng and J. Dong, Phys. Rev. B **73**, 132410 (2006).